Water Oxidation

DOI: 10.1002/anie.201406983

Homogeneous Electrocatalytic Water Oxidation at Neutral pH by a Robust Macrocyclic Nickel(II) Complex**

Mei Zhang, Ming-Tian Zhang, Cheng Hou, Zhuo-Feng Ke, and Tong-Bu Lu**

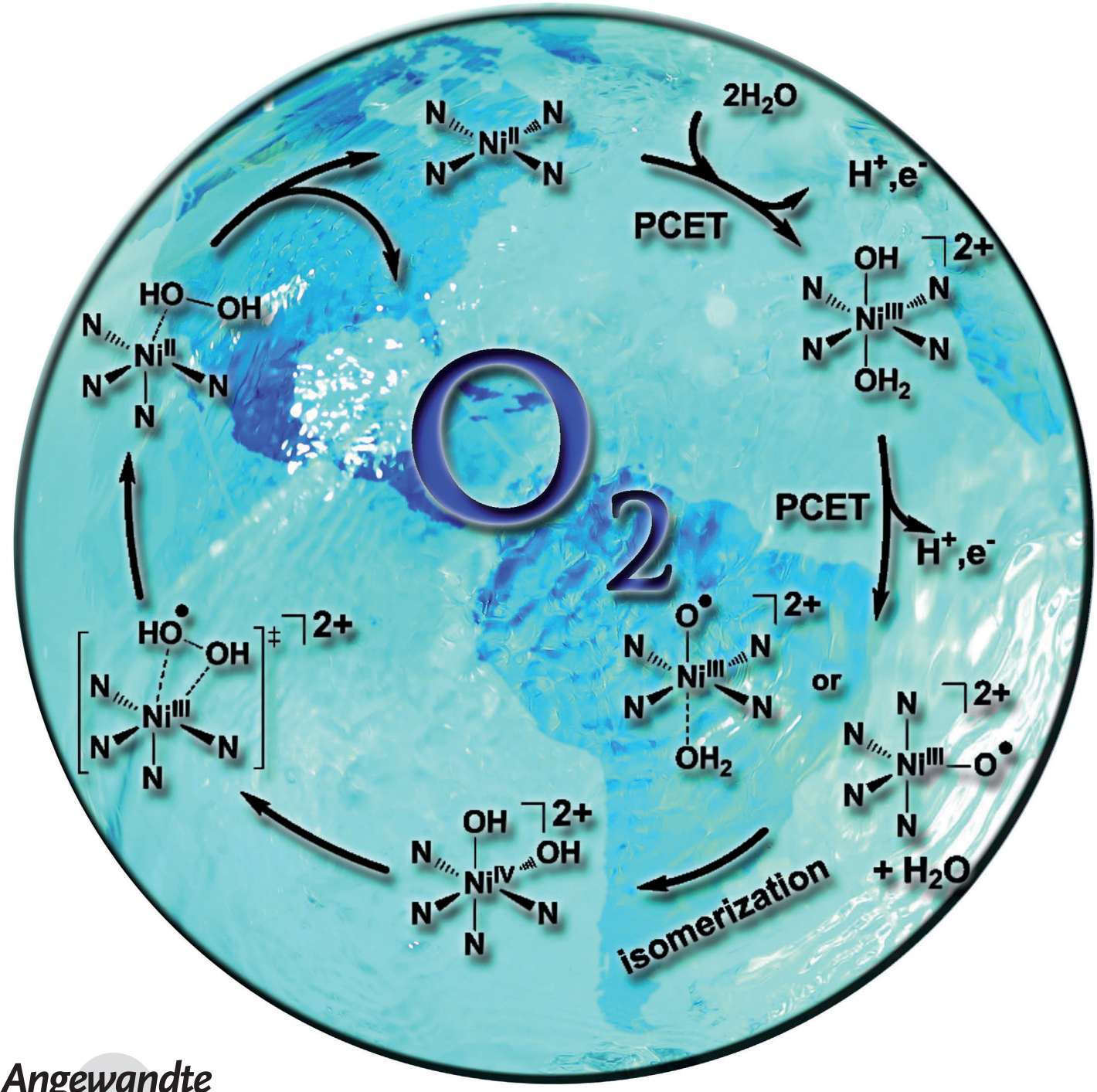

Abstract: *The development of an earth-abundant, first-row water oxidation catalyst that operates at neutral pH and low overpotential remains a fundamental chemical challenge. Herein, we report the first nickel-based robust homogeneous water oxidation catalyst, which can electrocatalyze water oxidation at neutral pH and low overpotential in phosphate buffer. The results of DFT calculations verify that the O−O bond formation in catalytic water oxidation prefers a HO−OH coupling mechanism from a cis-isomer of the catalyst.*

Water splitting continues to attract much attention for the purpose of producing hydrogen, which is regarded as the most promising alternative energy source for its cleanness, effectiveness and renewability.[1] Water splitting consists of two half reactions, the reduction of protons and the oxidation of water. The water oxidation reaction requires a multielectron transfer process along with a very high redox potential. This half reaction is considered as the bottleneck in overall water splitting,[2] because the water oxidation catalysts (WOCs) are easily decomposed and/or deactivated under the highly oxidizing conditions required to oxidize water. Thus, the development of robust and long-living WOCs has become a major challenge for the design of water splitting devices.[3]

Extensive efforts have been devoted to the development of water oxidation catalysts. Up to now, earth-scarce Ru[4] and Ir[5] WOCs have shown high water oxidation efficiencies. For example, Sun et al. reported a series of Ru WOCs[4d–h] which exhibit impressive catalytic activity for water oxidation, with an oxygen generation rate greater than 300 s^{-1}.[4g] While the high costs of Ru and Ir restricts their use on a large scale, WOCs based on earth-abundant elements such as Mn,[6] Fe,[7] Co,[8] Ni,[9] and Cu[10] have been extensively studied recently. However, beyond the Mn_4O_4Ca WOC in photosystem II, most WOCs including first-row metal complexes and oxides operate under basic or acidic conditions, while only few operate at neutral pH.[8g,10c,11] The development of an earth-abundant, first-row catalyst that operates at neutral pH and low overpotential remains a fundamental challenge.[8g]

Among water oxidation catalysts, homogeneous catalysts are advantageous because of their controllable redox properties. The characterization of active intermediates as well as mechanistic studies[8b,10c] and the resulting understanding is beneficial for the development of new catalysts.[10c] Up to now, homogeneous WOCs of Ru,[4d–h] Mn,[6c] Fe,[7c,d] Co[8b] and Cu[10] have been reported. However, to the best of our knowledge, no homogeneous nickel WOC has been reported so far. In addition, most reported water splitting catalysts can only catalyze one of two half reactions of water splitting, few catalysts can catalyze both water oxidation and proton reduction. It has been reported that a macrocyclic nickel(II) complex [Ni(*meso*-L)]$(ClO_4)_2$ (L = 5,5,7,12,12,14-hexamethyl-1,4,8,11-tetraazacyclotetradecane) can electrocatalyze water reduction to produce H_2 (Figure 1).[12] We were interested to see if this complex could also catalyze water oxidation to produce oxygen. Thus the electrocatalytic properties of [Ni(*meso*-L)]$(ClO_4)_2$ for water oxidation was investigated, and the results indicate that [Ni(*meso*-L)]$(ClO_4)_2$ can indeed electrocatalyze water oxidation at neutral pH and low overpotential. The results of electrochemical, spectroscopic and surface analysis demonstrate [Ni(*meso*-L)]$(ClO_4)_2$ is a homogeneous WOC.

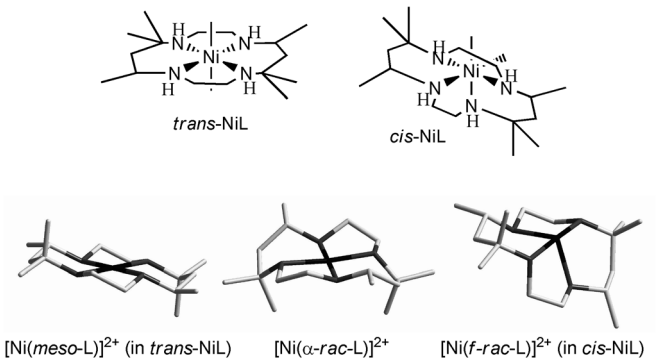

Figure 1. The structures of [Ni(*meso*-L)]$^{2+}$, [Ni(α-*rac*-L)]$^{2+}$ and [Ni(*f*-*rac*-L)]$^{2+}$.

The structures of [Ni(*meso*-L)]$^{2+}$ have been extensively investigated, and both four-coordinated [Ni(*meso*-L)]$^{2+}$[13] and six-coordinated [(*meso*-L)Ni$(OH_2)_2$]$^{2+}$[14] were isolated from aqueous solution. In the structure of six-coordinated [(*meso*-L)Ni$(OH_2)_2$]$^{2+}$, two water molecules are located at axial positions of Ni^{II}.[14] It has also been reported that there is an equilibrium between four-coordinated [Ni(*meso*-L)]$^{2+}$ and six-coordinated [(*meso*-L)Ni$(OH_2)_2$]$^{2+}$ in aqueous solution, in which a small amount of [(*meso*-L)Ni$(OH_2)_2$]$^{2+}$ coexists with [Ni(*meso*-L)]$^{2+}$.[15]

Figure 2 shows cyclic voltammograms (CVs) of [Ni^{II}(*meso*-L)]$(ClO_4)_2$ obtained on a glassy carbon (GC) electrode (0.071 cm^2) with the addition of 1 mM [Ni^{II}(*meso*-L)]$(ClO_4)_2$ in 0.1M sodium phosphate buffer (NaPi) at pH 7.0. Potentials were measured versus a saturated calomel electrode and are reported versus the normal hydrogen electrode (NHE). From Figure 2 it can be seen that there is a small irreversible oxidation wave at 0.87 V in the CV of [Ni^{II}(*meso*-L)]$(ClO_4)_2$ which can be assigned to the oxidation of Ni^{II} to Ni^{III}.[16] In addition, this oxidation wave is pH-dependent (Figure S1 in the Supporting Information), with the anodic peak potential versus pH decreasing by 59 mV per pH unit (Figure S2),

[*] M. Zhang, C. Hou, Prof. Z.-F. Ke, Prof. T.-B. Lu
MOE Key Laboratory of Bioinorganic and Synthetic Chemistry
State Key Laboratory of Optoelectronic Materials and Technologies
School of Chemistry and Chemical Engineering
Sun Yat-Sen University
Guangzhou 510275 (China)
E-mail: kezhf3@mail.sysu.edu.cn
lutongbu@mail.sysu.edu.cn
Dr. M.-T. Zhang
Center of Basic Molecular Science (CBMS)
Department of Chemistry, Tsinghua University
Beijing 100084 (China)

[**] This work was supported by the 973 Program of China (2012CB821706, 2014CB845602), the NSFC (grant nos. 21331007, 21121061, and 21203256), and the NSF of Guangdong Province (S2012030006240).

Supporting information for this article is available on the WWW under http://dx.doi.org/10.1002/anie.201406983.

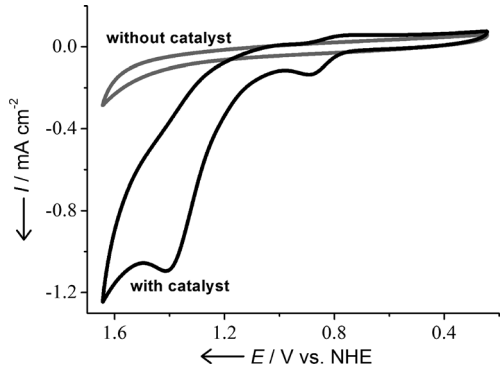

Figure 2. Cyclic voltammograms of 0 mM (gray line) and 1 mM (black line) [Ni(*meso*-L)]$(ClO_4)_2$ in 0.1 M phosphate buffer (pH 7.0, $I = 0.22$ M) at a GC electrode. Scan rate = 100 mV s^{-1}.

indicating the oxidation of Ni^{II} to Ni^{III} proceeds through a proton-coupled electron transfer (PCET) to give the hydroxy form [Eq. (1)]:

$$[(meso\text{-}L)Ni^{II}]^{2+} + 2H_2O \xrightarrow{-e^-,\,-H^+} [(meso\text{-}L)(H_2O)Ni^{III}(OH)]^{2+} \quad \text{or}$$
$$[(meso\text{-}L)Ni^{II}(OH_2)_2]^{2+} \xrightarrow{-e^-,\,-H^+} [(meso\text{-}L)(H_2O)Ni^{III}(OH)]^{2+} \quad (1)$$

At more positive potentials an additional irreversible oxidation wave at the oxidation current peak ($E_{p,a}$) of 1.41 V appears, with a drastically enhanced current above the background, consistent with catalytic water oxidation. The onset potential ($E_{p,o}$) for water oxidation emerges at ca. 0.99 V vs NHE, with an overpotential of only ca. 170 mV. This overpotential is much lower than the typical overpotentials for many homogeneous WOCs (300–600 mV).[8b,10] The second irreversible oxidation wave at 1.41 V can be attributed to the further oxidation from Ni^{III} to Ni^{IV} species, and it has been reported the potential of Ni^{IV}/Ni^{II} can exceed 1.6 V.[17] It is interesting to note that the peak potential for the second oxidation wave is also pH-dependent, with $E_{p,a}$ versus pH decreasing by 59 mV per pH unit (Figure S1 and S2), indicating the irreversible oxidation from Ni^{III} to Ni^{IV} also proceeds through a PCET. Thus, the product of the second oxidation would be a $[(meso\text{-}L)(H_2O)Ni^{IV}{=}O]^{2+}$ or $[(meso\text{-}L)(H_2O)Ni^{III}\text{-}O^{\bullet}]^{2+}$ intermediate [Eq. (2)]:

$$[(meso\text{-}L)(H_2O)Ni^{III}(OH)]^{2+} \xrightarrow{-e^-,\,-H^+} [(meso\text{-}L)(H_2O)Ni^{IV}{=}O]^{2+} \quad \text{or}$$
$$[(meso\text{-}L)(H_2O)Ni^{III}\text{-}O^{\bullet}]^{2+} \quad (2)$$

It has been found that the Ni^{IV} derivative favors a direct 2e reduction to Ni^{II} rather than through a Ni^{III} intermediate.[18] This is the origin of the irreversible oxidation wave for $[(meso\text{-}L)(H_2O)Ni^{III}(OH)]^{2+}$ appearing at 1.41 V in the CV of $[Ni^{II}(meso\text{-}L)](ClO_4)_2$ (Figure 2), in which the generated $[(meso\text{-}L)(H_2O)Ni^{IV}{=}O]^{2+}$ or $[(meso\text{-}L)(H_2O)Ni^{III}\text{-}O^{\bullet}]^{2+}$ intermediate was directly reduced to Ni^{II} species by water. In addition, the catalytic current density for water oxidation at 1.41 V increases linearly with the concentrations of $[Ni^{II}(meso\text{-}L)](ClO_4)_2$ (Figure S3), demonstrating a single-site nickel catalysis. Moreover, addition of 1 mM $Ni(NO_3)_2$ to 0.1 M NaPi buffer generated immediate precipitation, and the resulting suspension/solution did not show water oxidation catalytic activity (Figure S4), demonstrating the water oxidation is attributed to the complex rather than free Ni^{II} in solution. Apart from the NaPi buffer system, $[Ni^{II}(meso\text{-}L)](ClO_4)_2$ can also catalyze water oxidation in other buffer systems (acetate, carbonate) at pH 7.0 (Figure S5).

To evaluate the catalytic efficiency, the production of dioxygen was monitored by controlled potential electrolysis at +1.55 V vs NHE on ITO electrode (1.5 cm^2, 6–7 Ω surface resistivity). The experiment was performed in a three-compartment gas-tight cell with 1 mM $[Ni^{II}(meso\text{-}L)](ClO_4)_2$ in 0.1 M NaPi buffer at pH 7.0 under an Ar atmosphere. O_2 formation in the headspace was measured by using a calibrated Ocean Optics FOXY probe.[8g,19] During the controlled potential electrolysis at +1.55 V, the background current in the absence of catalyst was negligibly small (Figure 3), while

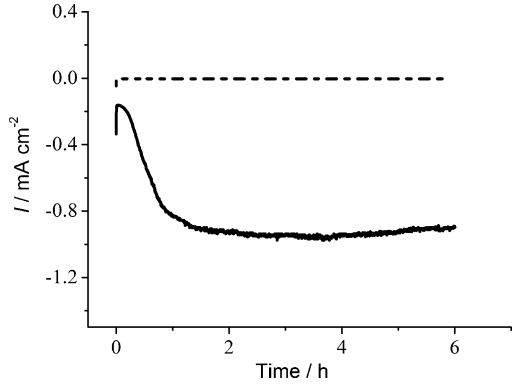

Figure 3. Catalytic current obtained at controlled potential electrolysis without stirring without (dotted line) and with (solid line) 1 mM [Ni(*meso*-L)]$(ClO_4)_2$ at an ITO electrode (1.5 cm^2) in 0.1 M phosphate buffer (pH 7.0) at 1.55 V vs NHE.

the catalytic current of the $[Ni^{II}(meso\text{-}L)](ClO_4)_2$ solution without stirring first increases slowly within 0–1 h, then becomes relatively stable to ca. 0.9 mA cm^{-2} upon further electrolysis (Figure 3). To understand why the catalytic current increases slowly within the first 1 h, the electrolysis was stopped for 1 min when the current became stable, then electrolysis was continued. It is interesting to note that the current almost recovered after the first 1-minute-stop (Figure S6), while after the second 1-minute-stop the current decreased and then slowly recovered within 8.6 min (Figure S6). For the third and fourth 1-min-stop it took 9.1 and 9.3 min for current recovery, respectively. In addition, the current rapidly decreased from 0.9 mA cm^{-2} to the initial current of 0.15 mA cm^{-2} after only 5 min of stopping electrolysis. On the other hand, with stirring the current maintains a value of 0.17 mA cm^{-2} and does not increase with increasing time of electrolysis (Figure S7). This value is much smaller than the current of 0.9 mA cm^{-2} observed without stirring. The above observation clearly demonstrates that the water

oxidation is achieved by an active intermediate which was slowly generated near the ITO electrode along with drastic conformation changes during the electrolysis, and this active intermediate rapidly transforms to a stable inactive species in solution (within 5 min). We attribute the active intermediate to a *cis*-isomer (*cis*-NiL, see Figure 1), which is slowly transformed from its *trans*-isomer of $[(meso\text{-L})(H_2O)Ni^{IV}{=}O]^{2+}$ or $[(meso\text{-L})(H_2O)Ni^{III}\text{-}O^{\bullet}]^{2+}$. Indeed, the ligand L exhibits several conformational isomers in $[NiL]^{2+}$, and the different isomers can interconvert in aqueous solution.[20] In addition, under the same conditions the electrolysis times during which the current increases to a stable value of 0.9 mA cm^{-2} can be shortened from 56 to 21 min when $[Ni(\alpha\text{-}rac\text{-L})]^{2+}$ was used as a catalyst instead of $[Ni(meso\text{-L})]^{2+}$ (Figure S8), indicating $[Ni(\alpha\text{-}rac\text{-L})]^{2+}$ is beneficial for the generation of the active intermediate, as $[Ni(\alpha\text{-}rac\text{-L})]^{2+}$ prefers a six-coordinated *cis*-NiL conformation in aqueous solution. The above observations demonstrate that isomerization from an inactive *trans*-isomer to an active *cis*-isomer may occur in solution during electrolysis. Costas and coworkers also found that six-coordinated Fe^{II} complexes possessing two *cis*-labile sites display high water oxidation activity, while those possessing two *trans*-labile sites are inactive for water oxidation.[7d] In addition, the normalized peak current ($i/v^{1/2}$) decreases with increasing scan rate (Figure S9), indicating the O–O bond formation is a rate-limiting step.[8b,10b] In addition, upon the addition of H_2O_2 to 1 mM $[Ni^{II}(meso\text{-L})](ClO_4)_2$ in 0.1 M sodium phosphate buffer (NaPi) at pH 7.0, the oxidation current of Ni^{II} to Ni^{III} on a GC electrode increased. The catalytic current increased with increasing concentrations of H_2O_2 (Figure S10), demonstrating that Ni^{III} can catalyze the oxidation of peroxide to O_2.

After electrolysis without stirring for 6 h, ca. 73 μmol of O_2 was detected (Figure 4), with a Faradaic efficiency of 97.5% and turnover number (TON) of 15 based on the initial amount of $[Ni(meso\text{-L})](ClO_4)_2$ in solution. After 6 h electrolysis, the CV, ESI-MS and UV/Vis spectrum of the resulting solution were measured (see Figures S11–S13). From Figures S11–S13 it can be seen that the CV, ESI-MS and UV/Vis spectra of the resulting solution are almost identical to those of the solution before electrolysis, indicating the $[Ni^{II}(meso\text{-L})](ClO_4)_2$ catalyst was not decomposed during electrolysis. In addition, the resulting solution after electrolysis was evaporated slowly at room temperature to obtain yellow crystals of $[Ni^{II}(meso\text{-L})](ClO_4)_2$ (Figure S14), which can be collected by hand. It is interesting to note that the $[Ni^{II}(meso\text{-L})](ClO_4)_2$ catalyst can be almost quantitatively recovered from the resulting solution after electrolysis, and the result of X-ray crystal structural analysis of the obtained yellow crystals indicates that the structure of the catalyst remains unchanged after electrolysis experiment (Figure S15), demonstrating the $[Ni^{II}(meso\text{-L})](ClO_4)_2$ catalyst is a robust and long-lived WOC. The high stability of $[Ni^{II}(meso\text{-L})](ClO_4)_2$ catalyst can be attributed to its low onset overpotential and water oxidation potential.

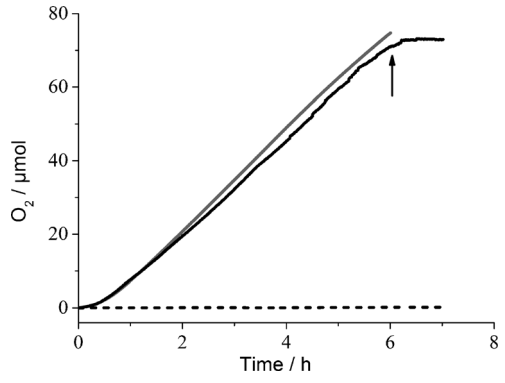

Figure 4. O_2 production measured by fluorescent sensor without (dotted line) and with (black solid line) 1 mM $[Ni(meso\text{-L})](ClO_4)_2$ without stirring at an ITO electrode (1.5 cm^2) in 0.1 M phosphate buffer (pH 7.0) at 1.55 V vs NHE. The gray solid line is the theoretical amount of O_2, with a Faradic efficiency of 97.5%. The arrow indicates termination of electrolysis.

To verify if the electrocatalysis by $[Ni^{II}(meso\text{-L})](ClO_4)_2$ is homogeneous or heterogeneous, consecutive scanning of 1 mM $[Ni^{II}(meso\text{-L})](ClO_4)_2$ at a GC electrode in 0.1 M NaPi buffer at pH 7.0 was performed. As shown in Figure S16, the catalytic current decreases along with continuous scanning and becomes almost constant after about 10 scan cycles. On the contrary, the CVs of the reported heterogeneous nickel-based catalysts[9b–d] show an increase in catalytic currents on repeated scanning, which is attributed to the deposition of nickel oxide (NiO_x) as water oxidation catalysts from the solution. The above different CV behavior prompts us to speculate that $[Ni^{II}(meso\text{-L})](ClO_4)_2$ is a homogeneous WOC. To further support this hypothesis, the GC electrode was rinsed with water several times after the above scans, but not polished. Then the electrode was cycled in fresh, catalyst-free electrolyte in 0.1 M NaPi buffer at pH 7.0. No significant catalytic current was observed relative to a freshly polished electrode (Figure S17), indicating the electrocatalysis of $[Ni^{II}(meso\text{-L})](ClO_4)_2$ on GC electrode is homogeneous.[10b,c] According to SEM measurements (Figure S18), after controlled potential electrolysis at +1.55 V for 6 h on ITO electrode no precipitation or film was deposited on the surface of the ITO electrode. Energy-dispersive X-ray spectroscopy (EDS) measurements also indicated no elemental Ni or P on the ITO surface (Figure S19). Dynamic laser scattering (DLS) found no significant nickel oxide nanoparticles generated in the solution after electrolysis. The above results demonstrate the electrocatalysis of $[Ni^{II}(meso\text{-L})](ClO_4)_2$ on either GC or ITO electrode is homogeneous.

Considering the nickel intermediates in high oxidation state are labile and may have various isomers, it is assumed that the electrocatalytic mechanism should be very complicated. We utilized DFT calculations to clarify the mechanism by evaluating all plausible intermediates and reaction pathways. Two PCET steps were both studied by DFT calculations, as shown in Figure S20. The first PCET from Ni^{II}-(*meso*-L), **Ni-1**, can lead to a *trans* octahedral Ni^{III} intermediate, $[(meso\text{-L})(H_2O)Ni^{III}(OH)]^{2+}$, ***trans*-Ni-2$_O$**, with a calculated PCET potential of 0.91 V. The isomerization may occur from ***trans*-Ni-2$_O$** to a five-coordinated trigonal-bipyramidal Ni^{III} intermediate, **Ni-2$_{TB}$**, accompanied with the dissociation of one water molecule (see Figure S20), as a d^7 Ni^{III} complex is usually a Jahn–Teller distorted octahedral or

five-coordinated species. However, the calculated PCET potential from **Ni-1** to **Ni-2$_{TB}$** is 1.30 V, which is much higher than the measured potential of 0.87 V. Therefore, the first PCET more likely proceeds from **Ni-1** to ***trans*-Ni-2$_O$**, as the calculated potential of 0.91 V is in good agreement with the measured potential of 0.87 V. The second PCET from ***trans*-Ni-2$_O$** will produce a Ni^{IV} intermediate ***trans*-Ni-3$_O$**, for which the calculated PCET potential is 1.74 V. The calculated redox potential is slightly higher than the measured potential (1.41 V) because the calculation ignores the effect of the buffer medium. However, the PCET from **Ni-2$_{TB}$** to **Ni-3$_{TB}$** cannot be entirely excluded. The calculation suggests that after isomerization from ***trans*-Ni-2$_O$** to **Ni-2$_{TB}$**, the subsequent PCET to **Ni-3$_{TB}$** requires a potential of 1.53 V, which is quite close to the measured potential of 1.41 V.

DFT calculations also provided interesting insights into the electronic structures and thermodynamic properties of the Ni^{IV} intermediates formed after the second PCET process. Calculations suggest that the formed Ni^{IV} intermediates should exist as various isomers in equilibriums. The *trans* octahedral ***trans*-Ni-3$_O$**, the *cis* octahedral ***cis*-Ni-3$_O$**, and the five-coordinated trigonal-bipyramidal **Ni-3$_{TB}$** intermediates are all thermodynamically accessible, as the free energy difference among these three isomers is only within 1.6 kcal mol^{-1} (Figure S20). Firstly, it is worth noting that a Ni^{IV}=O oxo species in ***trans*-Ni-3$_O$** is calculated to be less probable, as the free energy for a singlet species is 7.9 kcal mol^{-1} higher than for a triplet species. The reason is that the π backbonding to the metal center is disfavored for a d^6 Ni^{IV} species, although metal oxo species are widely suggested in metal-catalyzed water oxidation.[4,6,7] The ***trans*-Ni-3$_O$** complex is more likely to be a triplet species $[(meso\text{-L})(H_2O)Ni^{III}\text{-}O^{\bullet}]^{2+}$, with a d^7 Ni^{III} center, where one spin resides at the oxygen atom and the other at the metal center (Figure S21). Similar proposed isomers between Cu^{IV}=O and Cu^{III}-O$^{\bullet}$ can also be found in Meyer's copper(II) polypeptide system for water oxidation.[10b] In addition, a water molecule can readily dissociate from ***trans*-Ni-3$_O$** to generate **Ni-3$_{TB}$** due to the d orbital degeneration of d^7 Ni^{III} center. For ***cis*-Ni-3$_O$** with two OH ligands, the most stable isomer is a singlet state (1.1 kcal mol^{-1}) rather than a triplet state (13.3 kcal mol^{-1}), which can be expected for a d^6 octahedral Ni^{IV} center. As for trigonal-bipyramidal **Ni-3$_{TB}$**, similar to ***trans*-Ni-3$_O$**, the most stable isomer is a triplet, while the singlet Ni^{IV}=O oxo species is less stable, also due to the disfavored π backbonding to the d^6 Ni^{IV} center.

With the understanding of $Ni^{IV/III}$ intermediates, we further studied the O–O bond formation mechanisms during the electrocatalysis. Intermetallic reactions have been excluded by our experimental results, as the reaction rate is first-order dependent on the concentration of nickel species. Therefore, the O–O bond formation should be promoted by monometallic ***trans*-Ni-3$_O$**, ***cis*-Ni-3$_O$**, or **Ni-3$_{TB}$**. There are three major mechanisms for the O–O bond formation (Figure S22): 1) HO–OH coupling, 2) water attack, and 3) O–H insertion. We evaluated all three O–O bond formation mechanisms (Figures S23–S25), and the favorite O–O bond formation pathway for each $Ni^{IV/III}$ isomer is shown in Figure 5.

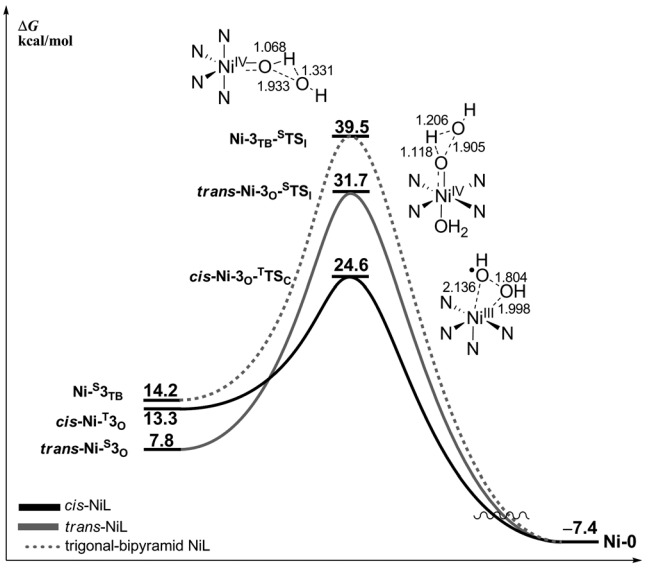

Figure 5. The calculated favorite O–O bond formation pathways for Ni^{IV} isomers. Bond lengths in transition states are in Å. The calculated Gibbs free energies are in kcal mol^{-1}.

Firstly, the most feasible O–O bond formation mechanism is found to be the HO–OH coupling from ***cis*-Ni-3$_O$** (transition state, ***cis*-Ni-3$_O$**; $\Delta G^{\neq} = 24.6$ kcal mol^{-1}). It is interesting to note this coupling prefers a triplet state over a singlet state ($\Delta G^{\neq} = 46.7$ kcal mol^{-1} from a singlet state intermediate, Figure S24), although the singlet ***cis*-Ni-3$_O$** is more stable. This is because the coupling transition state adopts a pseudo-trigonal-bipyramid geometry, in which the ligand field tends to be high spin. Secondly, a typical water attack mechanism is less possible ($\Delta G^{\neq} \approx 32.0$ kcal mol^{-1}, Figures S23, S25–S27). This is consistent with our former analysis that the electrophilic Ni^{IV} oxo intermediates are unstable. Thirdly, an insertion of singlet Ni^{IV}=O into the O–H bond of water is also predicted to be difficult ($\Delta G^{\neq} = 31.7$ and 39.5 kcal mol^{-1} for ***trans*-Ni-3$_O$** and **Ni-3$_{TB}$**, respectively, Figures 5, S23 and S25). Lastly, another O–H insertion pathway promoted by the Ni^{III}-O$^{\bullet}$ in triplet ***trans*-Ni-3$_O$** or **Ni-3$_{TB}$** is even more difficult ($\Delta G^{\neq} > 40$ kcal mol^{-1}, Figure S23 and S25). Therefore, the DFT calculations support that the O–O bond formation prefers a HO–OH coupling mechanism from *cis*-isomer $[(f\text{-}rac\text{-L})(HO)Ni^{III}(^{\bullet}OH)]^{2+}$.

Based on the above experimental observations and DFT studies a proposed mechanism for $[Ni^{II}(meso\text{-L})](ClO_4)_2$-mediated water oxidation is shown in Figure 6. First, $[(meso\text{-L})Ni^{II}]^{2+}$ is oxidized through a PCET to give a *trans* octahedral Ni^{III} intermediate, $[(meso\text{-L})(H_2O)Ni^{III}(OH)]^{2+}$, ***trans*-Ni-2$_O$** [Eq. (1)], which is further oxidized through an additional PCET to give ***trans*-Ni-3$_O$** ($[(meso\text{-L})(H_2O)Ni^{III}\text{-}O^{\bullet}]^{2+}$, [Eq. (1)]). Then ***trans*-Ni-3$_O$** slowly isomerizes to its *cis*-isomer, ***cis*-Ni-3$_O$** ($[(f\text{-}rac\text{-L})(HO)Ni^{IV}(OH)]^{2+}$ or $[(f\text{-}rac\text{-L})(HO)Ni^{III}(^{\bullet}OH)]^{2+}$), and the O–O bond is formed through a HO–OH coupling pathway to generate $[(f\text{-}rac\text{-L})Ni^{II}(HOOH)]^{2+}$ intermediate through a $[(f\text{-}rac\text{-L})Ni^{III}(HO\cdots OH)]^{2+}$ transition state. $[(f\text{-}rac\text{-L})Ni^{II}(HOOH)]^{2+}$ intermediate is further oxidized to produce O_2. To our knowledge,

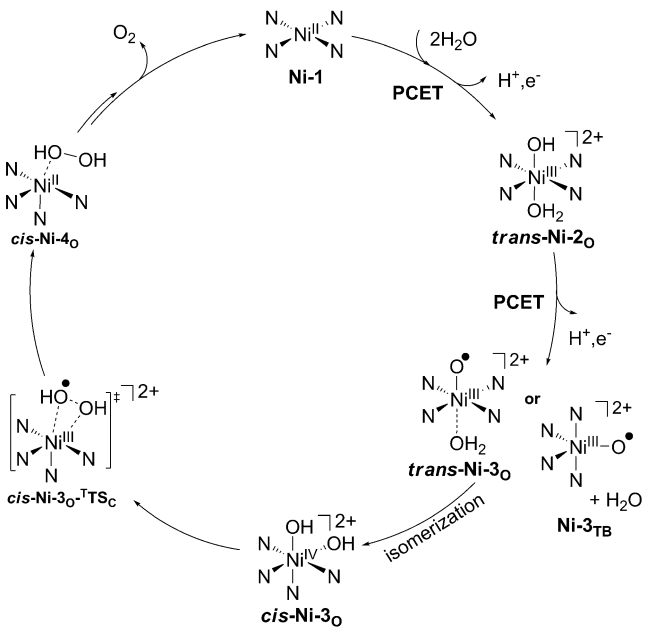

Figure 6. The proposed mechanism for water oxidation by $[Ni^{II}(meso\text{-}L)](ClO_4)_2$ via HO–OH coupling at neutral pH.

a similar water oxidation pathway has not been reported so far.

In summary, we report here the first homogeneous nickel-based electrocatalyst for water oxidation. The $[Ni^{II}(meso\text{-}L)](ClO_4)_2$ catalyst shows the following unusual features: First, it is an earth-abundant, first-row, robust and homogeneous catalyst that can oxidize water at pH 7 and low overpotential. Second, it can electrocatalyze both water oxidation and proton reduction. The active intermediate for water oxidation is ***cis*-Ni-3$_O$**, which is formed by isomerization from ***trans*-Ni-3$_O$**, and the *cis*-conformation of ***cis*-Ni-3$_O$** is the key factor for the HO–OH coupling to form the O–O bond. In comparison with homogeneous Ru WOCs, the catalytic activity of $[Ni^{II}(meso\text{-}L)](ClO_4)_2$ for water oxidation is relatively low, probably due to the drastic conformation change from the inactive *trans*-conformation to the active *cis*-conformation during water oxidation. We consider the catalytic activity could be improved using a six-coordinated Ni^{II} complex possessing two *cis* labile sites, as *cis*-conformation is beneficial for the HO–OH coupling. In the next step, we will synthesize such a Ni complex to improve the catalytic activity of Ni-based homogeneous WOCs.

Received: July 7, 2014
Published online: September 9, 2014

Keywords: electrocatalysis · homogeneous water oxidation · HO–OH coupling · nickel

[1] a) J. R. Swierk, T. E. Mallouk, *Chem. Soc. Rev.* **2013**, *42*, 2357 – 2387; b) M. Wang, L. Chen, L. Sun, *Energy Environ. Sci.* **2012**, *5*, 6763 – 6778.

[2] M. D. Kärkäs, T. Åkermark, H. Chen, J. Sun, B. Åkermark, *Angew. Chem. Int. Ed.* **2013**, *52*, 4189 – 4193; *Angew. Chem.* **2013**, *125*, 4283 – 4287.

[3] K. S. Joya, Y. F. Joya, K. Ocakoglu, R. van de Krol, *Angew. Chem. Int. Ed.* **2013**, *52*, 10426 – 10437; *Angew. Chem.* **2013**, *125*, 10618 – 10630.

[4] a) L. Wang, L. Duan, B. Stewart, M. Pu, J. Liu, T. Privalov, L. Sun, *J. Am. Chem. Soc.* **2012**, *134*, 18868 – 18880; b) J. J. Concepcion, J. W. Jurss, J. L. Templeton, T. J. Meyer, *J. Am. Chem. Soc.* **2008**, *130*, 16462 – 16463; c) D. E. Polyansky, J. T. Muckerman, J. Rochford, R. Zong, R. P. Thummel, E. Fujita, *J. Am. Chem. Soc.* **2011**, *133*, 14649 – 14665; d) F. Li, Y. Jiang, B. Zhang, F. Huang, Y. Gao, L. Sun, *Angew. Chem. Int. Ed.* **2012**, *51*, 2417 – 2420; *Angew. Chem.* **2012**, *124*, 2467 – 2470; e) Y. Jiang, F. Li, B. Zhang, X. Li, X. Wang, F. Huang, L. Sun, *Angew. Chem. Int. Ed.* **2013**, *52*, 3398 – 3401; *Angew. Chem.* **2013**, *125*, 3482 – 3485; f) Y. Gao, X. Ding, J. Liu, L. Wang, Z. Lu, L. Li, L. Sun, *J. Am. Chem. Soc.* **2013**, *135*, 4219 – 4222; g) L. Duan, F. Bozoglian, S. Mandal, B. Stewart, T. Privalov, A. Llobet, L. Sun, *Nat. Chem.* **2012**, *4*, 418 – 423; h) F. Li, B. Zhang, X. Li, Y. Jiang, L. Chen, Y. Li, L. Sun, *Angew. Chem. Int. Ed.* **2011**, *50*, 12276 – 12279; *Angew. Chem.* **2011**, *123*, 12484 – 12487.

[5] a) N. D. Schley, J. D. Blakemore, N. K. Subbaiyan, C. D. Incarvito, F. D'Souza, R. H. Crabtree, G. W. Brudvig, *J. Am. Chem. Soc.* **2011**, *133*, 10473 – 10481; b) J. D. Blakemore, N. D. Schley, D. Balcells, J. F. Hull, G. W. Olack, C. D. Incarvito, O. Eisenstein, G. W. Brudvig, R. H. Crabtree, *J. Am. Chem. Soc.* **2010**, *132*, 16017 – 16029; c) J. F. Hull, D. Balcells, J. D. Blakemore, C. D. Incarvito, O. Eisenstein, G. W. Brudvig, R. H. Crabtree, *J. Am. Chem. Soc.* **2009**, *131*, 8730 – 8731.

[6] a) D. M. Robinson, Y. B. Go, M. Mui, G. Gardner, Z. Zhang, D. Mastrogiovanni, E. Garfunkel, J. Li, M. Greenblatt, G. C. Dismukes, *J. Am. Chem. Soc.* **2013**, *135*, 3494 – 3501; b) T. Takashima, K. Hashimoto, R. Nakamura, *J. Am. Chem. Soc.* **2012**, *134*, 18153 – 18156; c) E. A. Karlsson, B.-L. Lee, T. Åkermark, E. V. Johnston, M. D. Kärkäs, J. Sun, Ö. Hansson, J.-E. Bäckvall, B. Åkermark, *Angew. Chem. Int. Ed.* **2011**, *50*, 11715 – 11718; *Angew. Chem.* **2011**, *123*, 11919 – 11922.

[7] a) G. Chen, L. Chen, S.-M. Ng, W.-L. Man, T.-C. Lau, *Angew. Chem. Int. Ed.* **2013**, *52*, 1789 – 1791; *Angew. Chem.* **2013**, *125*, 1833 – 1835; b) J. A. Seabold, K.-S. Choi, *J. Am. Chem. Soc.* **2012**, *134*, 2186 – 2192; c) W. C. Ellis, N. D. McDaniel, S. Bernhard, T. J. Collins, *J. Am. Chem. Soc.* **2010**, *132*, 10990 – 10991; d) J. L. Fillol, Z. Codolà, I. Garcia-Bosch, L. Gómez, J. J. Pla, M. Costas, *Nat. Chem.* **2011**, *3*, 807 – 813.

[8] a) C. A. Kent, J. J. Concepcion, C. J. Dares, D. A. Torelli, A. J. Rieth, A. S. Miller, P. G. Hoertz, T. J. Meyer, *J. Am. Chem. Soc.* **2013**, *135*, 8432 – 8435; b) D. Wang, J. T. Groves, *Proc. Natl. Acad. Sci. USA* **2013**, *110*, 15579 – 15584; c) R. D. L. Smith, M. S. Prévot, R. D. Fagan, S. Trudel, C. P. Berlinguette, *J. Am. Chem. Soc.* **2013**, *135*, 11580 – 11586; d) T. Zidki, L. Zhang, V. Shafirovich, S. V. Lymar, *J. Am. Chem. Soc.* **2012**, *134*, 14275 – 14278; e) Y. Surendranath, D. A. Lutterman, Y. Liu, D. G. Nocera, *J. Am. Chem. Soc.* **2012**, *134*, 6326 – 6336; f) D. K. Dogutan, R. McGuire, D. G. Nocera, *J. Am. Chem. Soc.* **2011**, *133*, 9178 – 9180; g) M. W. Kanan, D. G. Nocera, *Science* **2008**, *321*, 1072 – 1075; h) Y. Surendranath, M. Dincă, D. G. Nocera, *J. Am. Chem. Soc.* **2009**, *131*, 2615 – 2620.

[9] a) D. K. Bediako, Y. Surendranath, D. G. Nocera, *J. Am. Chem. Soc.* **2013**, *135*, 3662 – 3674; b) A. Singh, S. L. Y. Chang, R. K. Hocking, U. Bach, L. Spiccia, *Catal. Sci. Technol.* **2013**, *3*, 1725 – 1732; c) A. Singh, S. L. Y. Chang, R. K. Hocking, U. Bach, L. Spiccia, *Energy Environ. Sci.* **2013**, *6*, 579 – 586; d) M. Dincă, Y. Surendranath, D. G. Nocera, *Proc. Natl. Acad. Sci. USA* **2010**, *107*, 10337 – 10341; e) D. K. Bediako, B. Lassalle-Kaiser, Y. Surendranath, J. Yano, V. K. Yachandra, D. G. Nocera, *J. Am. Chem. Soc.* **2012**, *134*, 6801 – 6809; f) D. C. Hong, Y. Yamada, T.

Nagatomi, Y. Takai, S. Fukuzumi, *J. Am. Chem. Soc.* **2012**, *134*, 19572 – 19575; g) G. Chen, L. J. Chen, S. M. Ng, T. C. Lau, *ChemSusChem* **2014**, *7*, 127 – 134.

[10] a) Z. Chen, T. J. Meyer, *Angew. Chem. Int. Ed.* **2013**, *52*, 700 – 703; *Angew. Chem.* **2013**, *125*, 728 – 731; b) M.-T. Zhang, Z. Chen, P. Kang, T. J. Meyer, *J. Am. Chem. Soc.* **2013**, *135*, 2048 – 2051; c) S. M. Barnett, K. I. Goldberg, J. M. Mayer, *Nat. Chem.* **2012**, *4*, 498 – 502.

[11] a) M. L. Rigsby, S. Mandal, W. Nam, L. C. Spencer, A. Llobet, S. S. Stahl, *Chem. Sci.* **2012**, *3*, 3058 – 3062; b) T. Zhang, C. Wang, S. Liu, J.-L. Wang, W. Lin, *J. Am. Chem. Soc.* **2013**, *136*, 273 – 281.

[12] B. J. Fisher, R. Eisenberg, *J. Am. Chem. Soc.* **1980**, *102*, 7361 – 7363.

[13] M. G. B. Drew, K. F. Mok, *Acta Crystallogr. Sect. C* **1987**, *43*, 666 – 668.

[14] Q. Zhang, X.-P. Shen, H. Zhou, *Acta Crystallogr. Sect. E* **2009**, *65*, m1141.

[15] E. Colacio, I. Ben Maimoun, R. Kivekäs, R. Sillanpää, J. Suárez-Varela, *Inorg. Chim. Acta* **2004**, *357*, 1465 – 1470.

[16] a) E. Zeigerson, G. Ginzburg, N. Schwartz, Z. Luz, D. Meyerstein, *J. Chem. Soc. Chem. Commun.* **1979**, 241 – 243; b) J. Schneider, H. Jia, K. Kobiro, D. E. Cabelli, J. T. Muckerman, E. Fujita, *Energy Environ. Sci.* **2012**, *5*, 9502 – 9510.

[17] R. Jurczakowski, G. Litwinienko, M. Orlik, *Z. Phys. Chem.* **2006**, *220*, 1083 – 1099.

[18] S. Mandal, E. S. Gould, *Inorg. Chem.* **1995**, *34*, 3993 – 3997.

[19] R. D. L. Smith, M. S. Prevot, R. D. Fagan, Z. Zhang, P. A. Sedach, M. K. J. Siu, S. Trudel, C. P. Berlinguette, *Science* **2013**, *340*, 60 – 63.

[20] L. Jiang, X. L. Feng, T. B. Lu, *Cryst. Growth Des.* **2005**, *5*, 1469 – 1475.

